Bolu Viaduct-1 Subjected to Near-Fault Ground Motion

by

Sunwoo Park[1], Hamid Ghasemi[2], Jerry Shen[1], and Phillip Yen[2]

ABSTRACT

The performance of seismically-isolated Bolu Viaduct-1 in Turkey subjected to a simulated near-fault ground motion during the 1999 Duzce Earthquake was evaluated through nonlinear finite element analysis. The ground motion is characterized by a large residual movement of the ground across the fault rupture that crosses the viaduct. Analysis indicates that the ground motion induces response that exceeds the design capacities of the seismic isolation systems thus resulting in substantial damage to the bearings and energy dissipation units, which is consistent with post-earthquake field observation. The analysis also indicates that shear keys, both longitudinal and transverse, play a critical role in preventing the superstructure collapse.

KEY WORDS: seismic isolation, damping, Viaduct 1, Duzce earthquake, near-fault

1.0 INTRODUCTION

Developments in seismic isolation and energy dissipation devices have permitted considerable advances in seismic protection of highway bridges. However, existing seismic protection strategies are largely based on design ground motions that do not contain near-fault features. Experience with a number of recent earthquakes has pointed to the need for accounting for the effects of near-fault ground motions in the seismic design of highway bridges. In this paper, the effects of a near-fault earthquake ground motion on the performance of a seismically isolated bridge are studied through numerical analysis of Bolu Viaduct 1 subjected to the 1999 Duzce Earthquake.

Bolu Viaduct 1 is located in north central Turkey and is part of the Trans-European Motorway (TEM) running from Ankara to Europe, see Figs 1 and 2. The 2.3-km viaduct, with its 59 dual spans, was approximately 95% complete at the time of the earthquake. The superstructure consists of seven lines of simply-supported, prestressed-concrete box girders seated on sliding bearings with stainless steel/PTFE slider interfaces. The deck slab is monolithic over 10-span segments and each segment is 392 m long and supported by 11 piers. An energy dissipation system of yielding-steel type is also installed on each pier cap to form, together with the sliding bearings, a seismic isolation system for the viaduct.

2.0 NUMERICAL ANALYSIS

Numerical simulation of the response of a typical ten-span segment of the viaduct subjected to a recorded and a simulated earthquake ground motion is conducted via nonlinear time-history analysis. The viaduct's superstructure and piers are modeled using 3-D beam elements, and the foundation conditions at each pier base are modeled by elastic translational and rotational springs. Special nonlinear link elements are used to model energy dissipation units (EDUs), sliding (or friction pot) bearings, and shear keys, see Fig. 3. The schematic illustration of the constitutive behavior of the nonlinear link elements used in the analysis are presented in Fig. 4. The force-displacement hysteretic behavior of the EDU resembles that of a lead-rubber bearing or friction pendulum system, and behavior of the sliding bearing is dictated by the coefficient of

[1] LENDIS Corporation @ Federal Highway Administration, Office of Infrastructure R&D, 6300 Georgetown Pike, McLean, VA 22101, USA
[2] Federal Highway Administration, Office of Infrastructure R&D, 6300 Georgetown Pike, McLean, VA 22101, USA

friction of the sliding surfaces. Seven bearings, each between a girder and pier cap, are modeled by a single bearing element, and multiple transverse shear keys are also modeled by a single gap/hook element, situated between the superstructure and pier. A pedestal for an EDU plays the role of a longitudinal shear key. The displacement capacity of the sliding bearings is 210 mm and the displacement capacities of the EDUs, longitudinal and transverse shear keys are all 480 mm, which presents apparent inconsistency.

A ground motion recorded at the Bolu station in the 1999 Duzce earthquake and a simulated near-fault ground motion are used as the input in the analysis. Figure 5 shows the acceleration histories and spectra of the two horizontal components of the Bolu ground motion. The design spectra shown is based on the 1999 AASHTO Guide Specifications for Seismic Isolation Design (AASHTO, 1999). An acceleration coefficient, A=0.4, and Soil Type II are assumed. The acceleration histories and spectra of the fault-normal and fault-parallel components of the simulated near-fault ground motion at the site of Viaduct 1 are shown in Fig. 6, and the corresponding ground displacement histories are presented in Fig. 7. It is to be noted that the effect of surface fault rupture that crosses the 10-span segment is modeled by specifying a different ground motion to each side of the segment divided by the rupture crossing as indicated in Fig. 8. The surface rupture is oriented at an approximate angle of 25° relative to the axis of the viaduct segment analyzed. The left-hand side of the segment in Fig. 8 is subjected to a motion defined by fault-normal and fault-parallel 1 components shown in Fig. 6, and the right-hand side is subjected to a motion defined by fault-normal and fault-parallel 2 components.

The two fault-parallel components are created by superimposing a pulse motion ("Type-A" by Makris and Chang, 2000) on the E-W component of the Bolu record, and the fault-normal component by superimposing a pulse motion ("Type-B" by Makris and Chang, 2000) on the N-S component of the Bolu record. The two fault-parallel components contain a pulse motion that induces a residual displacement of 0.75 m in opposite directions (representing "fling" effect), thus resulting in a relative displacement of 1.5 m across the surface rupture, see Fig. 7. The ground motions applied to either side of the segment have the same fault-normal component due to kinematic continuity across the fault rupture, and the magnitude of the fault-normal component is estimated from its conjugate relationship to the fault-parallel component in a related problem (Anderson and Luco, 1983). The simulated near-fault ground motion uses the Bolu record as the background far-field motion and is consistent with the field observation of an approximate relative ground movement of 1.5 m across the surface rupture.

3.0 RESULTS OF ANALYSIS

Analysis has focused on the displacement of isolation/damping elements. The bearing displacement at the center pier of the 10-span segment subjected to the Bolu ground motion is shown in Fig. 9. It is to be noted that the displacement of bearing (or EDU) represents the relative displacement between the superstructure and pier. The time histories of the longitudinal and transverse components are shown in Figs. 9(a) and (b), respectively, and the displacement path on the bearing surface in Fig. 9(c). The displacement capacities of sliding bearings and shear keys are indicated in broken lines in Fig. 9(c). It can be seen that the bearing's displacement capacity is exceeded at an early stage of the movement. It is believed that, due to this exceedance, EDUs are distorted and failed before they can be functioned as designed. Post-earthquake field investigations have revealed that the majority of the EDUs were broken for the 10-span segment which was crossed by the fault rupture. In our analysis, different levels of EDU survival were considered, and the results shown in Figs. 9 to 11 are all based on the assumption that the entire EDUs are failed at the beginning. Figure 9 indicates that, while the longitudinal shear key was briefly engaged, the transverse shear key has never been engaged under the Bolu ground motion. Field inspections revealed that transverse as well as longitudinal shear keys of Viaduct 1 were repeatedly engaged during the earthquake. It is believed that the

Bolu ground motion does not induce the observed damage to the viaduct, suggesting that a much stronger near-fault ground motion must have hit the Viaduct 1 site in the 1999 Duzce earthquake.

Figures 10 and 11 respectively show the bearing displacements at the pier immediately left (P1 in Fig. 8) and immediately right (P2 in Fig. 8) of the fault rupture under the simulated near-fault ground motion. The displacement capacity of the sliding bearings is exceeded during the first major cycle of movement, and then both longitudinal and transverse shear keys are engaged. Analysis indicates that the longitudinal shear keys at both piers remain engaged after the event due to the large relative ground movement across the fault rupture, and that the transverse shear key at P1 remain engaged following several interactions between the girder and shear key. The displacement demand due to the static ground movement (1.5 m) is accommodated partly by bearings (until the longitudinal shear key is engaged) and partly by the pier. It is interesting to note that the shear keys, both longitudinal and transverse, are engaged only on one side throughout the motion, which is consistent with findings from field inspection of the shear keys.

Finally, post-earthquake field reconnaissance survey has revealed that the majority of the stainless steel interface plates had distinct scoring that resembled the number “9” as shown in Fig. 12(a) (Ghasemi et al., 2000). The calculated displacement path as shown in Fig. 12(b) is fairly consistent with the field observation. The initial movement consists of a half cycle of displacement with an amplitude of approximately 130 mm followed by movement in the opposite direction that exceeds the bearing’s displacement capacity. Due to this exceedance at an early stage of the ground motion, subsequent large movement of the girders (which are already dropped off the bearing plates) on pier-cap table is believed to have caused damage to sliding bearings (including ejection of bearing plates) and EDUs and, as a consequence, the entire seismic isolation/damping systems did not function as designed. However, from a technical point of view, the viaduct performed satisfactorily largely due to shear keys (longitudinal and transverse) that prevented collapse of the superstructure segments.

4.0 CONCLUSIONS

Analysis of the seismically-isolated Viaduct 1 subjected to the ground motion recorded at the Bolu station resulted in displacements exceeding the capacity of the isolation bearings but not large enough to engage shear keys and to cause significant damage to the viaduct as was observed in the post-earthquake investigation. However, analysis with a simulated near-fault ground motion that accounts for relative static ground movement across the surface rupture resulted in displacements far exceeding the capacities of the isolation bearings and EDUs and resulted in engagement of the shear keys, both longitudinal and transverse. The calculated bearing displacement paths are consistent with the “9”-shaped scoring trace observed on the surface of the bearing plates at the site. The close proximity of the fault rupture to the viaduct caused significant superstructure movement relative to the piers resulting in severe damage to bearings, EDUs, and shear keys. The simulation, however, indicates that the shear keys played a critical role in preventing superstructure segments from dropping off the pier caps thus preventing a collapse of the viaduct during the earthquake.

5.0 REFERENCES

AASHTO (1999). *Guide Specifications for Seismic Isolation Design*. American Association of State Highway and Transportation Officials, Washington, DC.

Anderson, J. G. and Luco, J. E. (1983). Parametric study of near-field ground motion for a strike-slip dislocation model. *Bulletin of the Seismological Society of America*, **73**(1), 23-43.

Makris, N. and Chang, S.-P. (2000). Effect of viscous, viscoplastic, and friction damping on the response of seismic isolated structures. *Earthquake Engineering and Structural Dynamics*, **29**, 85-107.

Ghasemi, H., Cooper, J. D., Imbsen, R., Piskin, H., Inal, F., and Tiras, A. (2000). *The November 1999 Duzce Earthquake: Post-Earthquake Investigation of the Structures on the TEM.* Publication No. FHWA-RD-00-146, Federal Highway Administration, U. S. Department of Transportation, Washington, D.C.

Fig.1. General area map.

Fig.2. General view of Bolu Viaduct 1

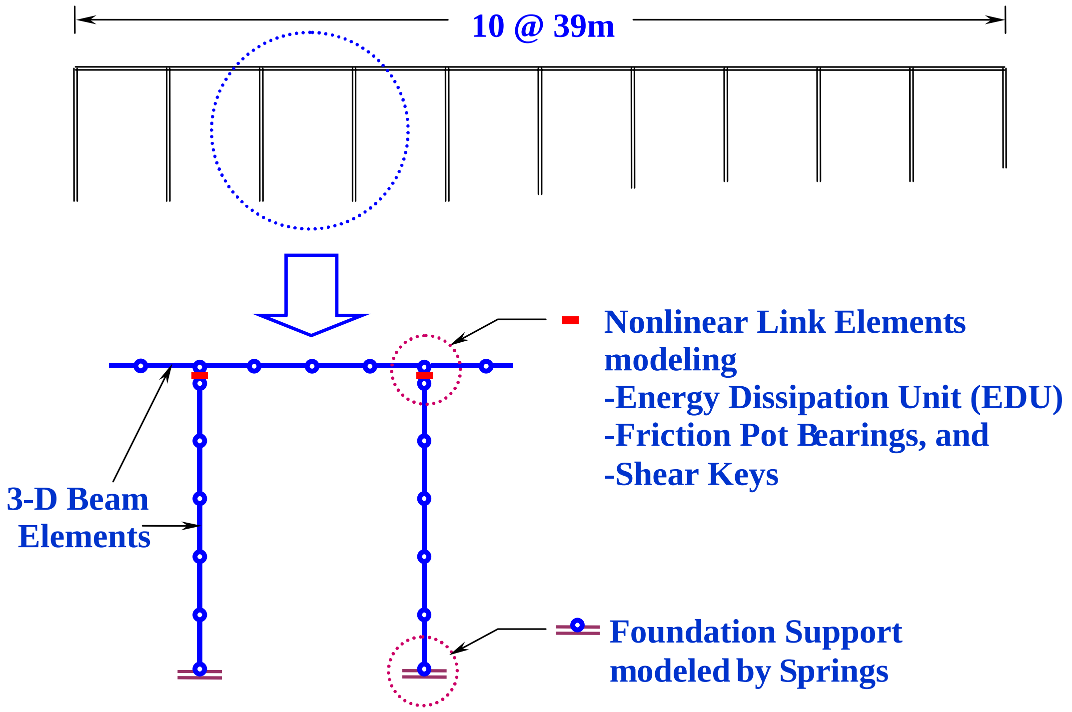

Fig. 3. Finite element discretization of a 10-span segment of Viaduct 1

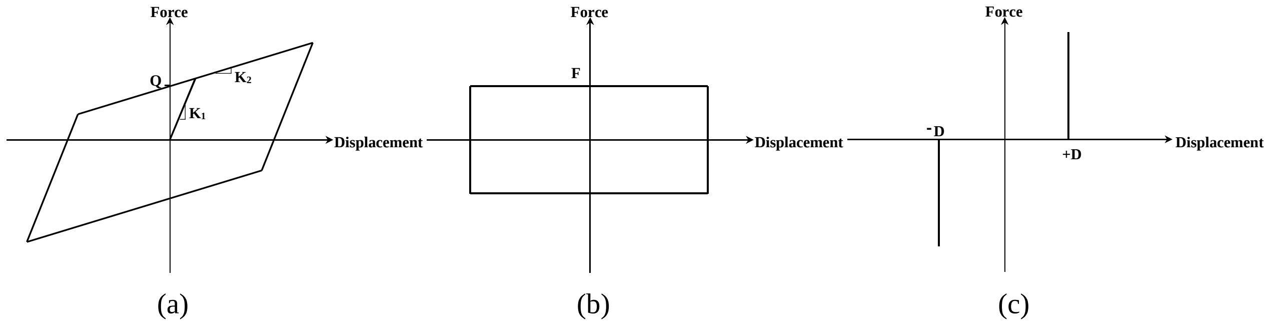

Fig. 4. Schematic illustration of constitutive models for (a) EDUs, (b) friction bearings, and (c) shear keys.

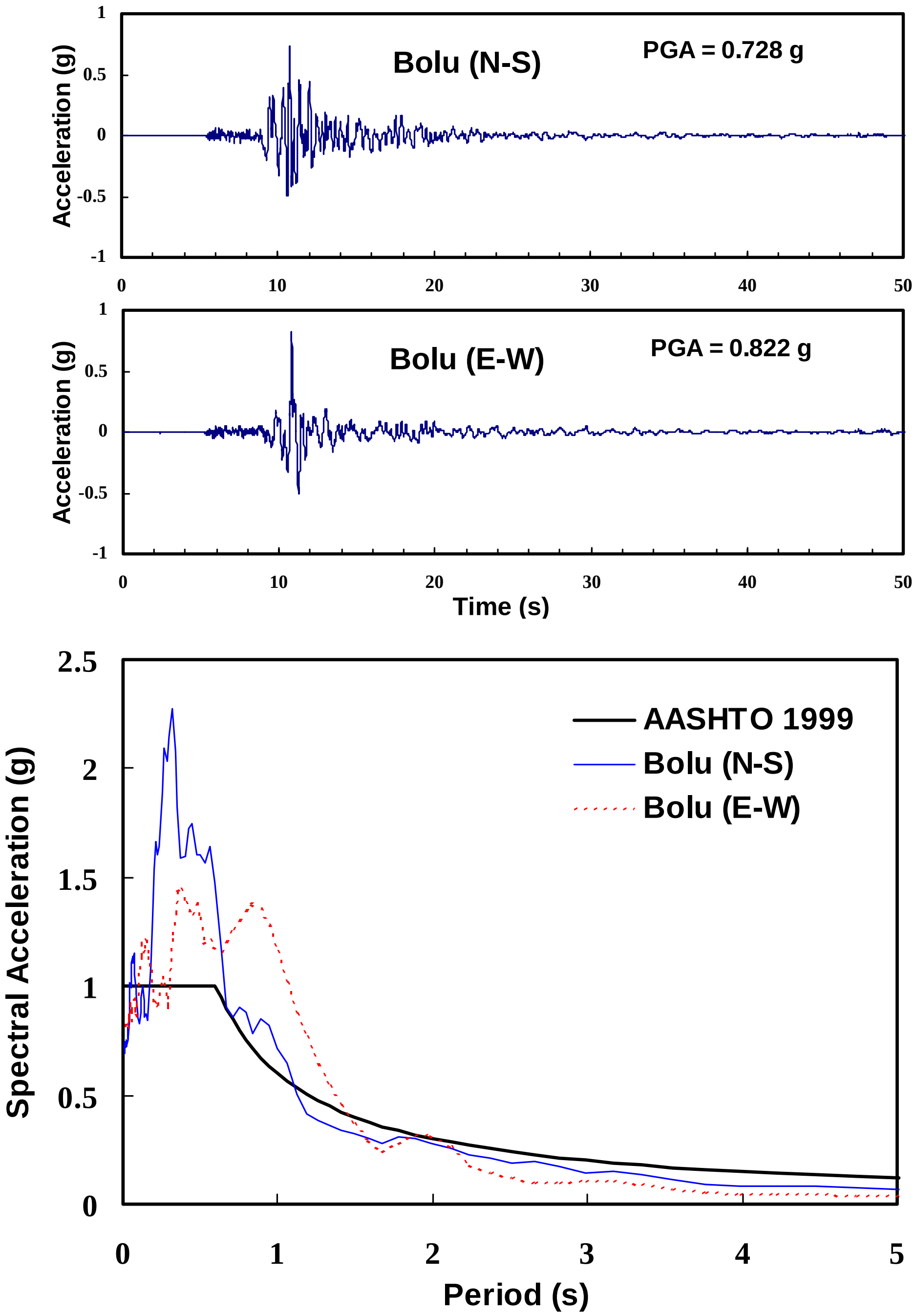

Fig. 5. Acceleration histories and spectra of the ground motion recorded at the Bolu station.

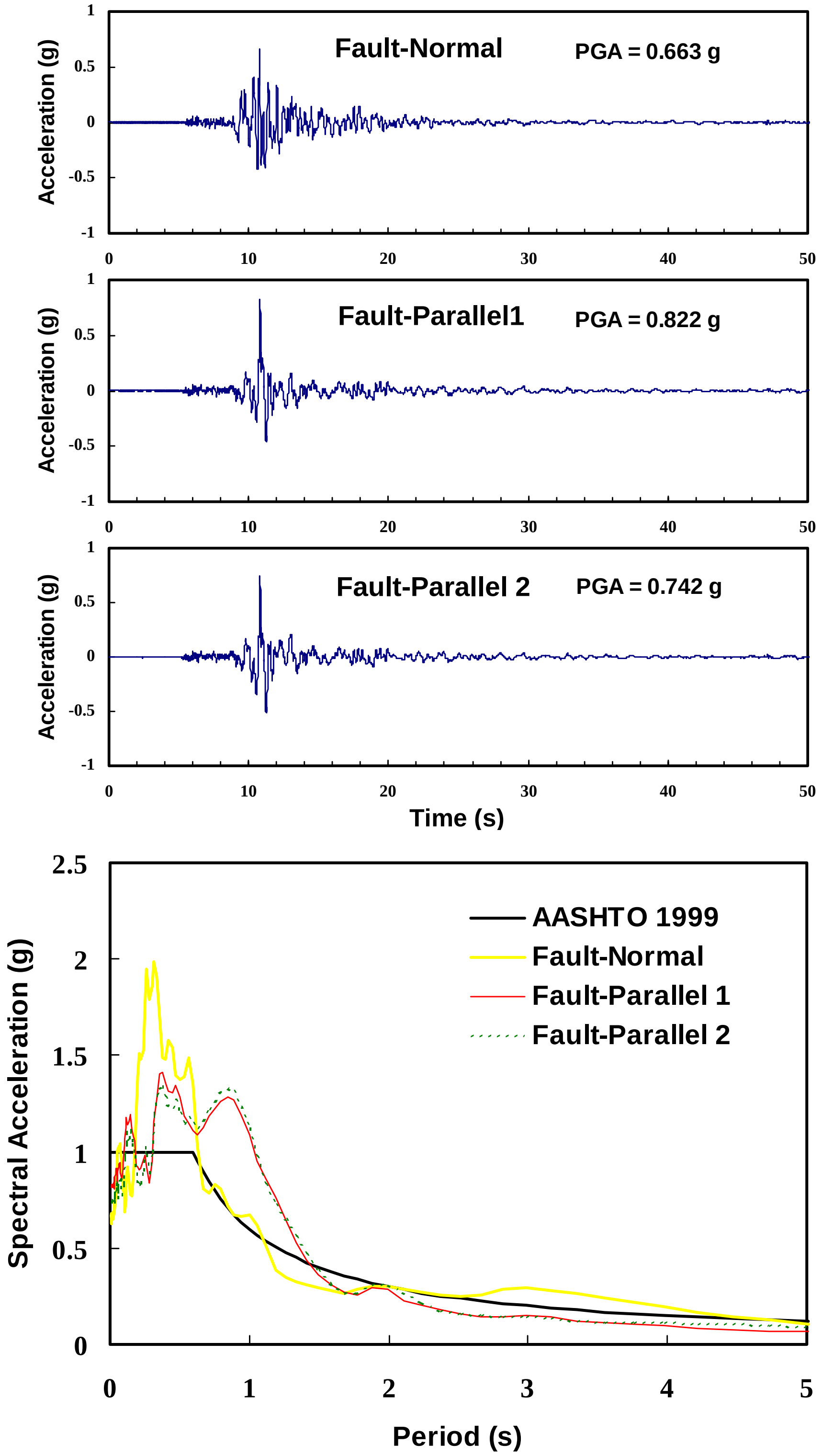

Fig. 6. Acceleration histories and spectra of the simulated near-fault ground motion.

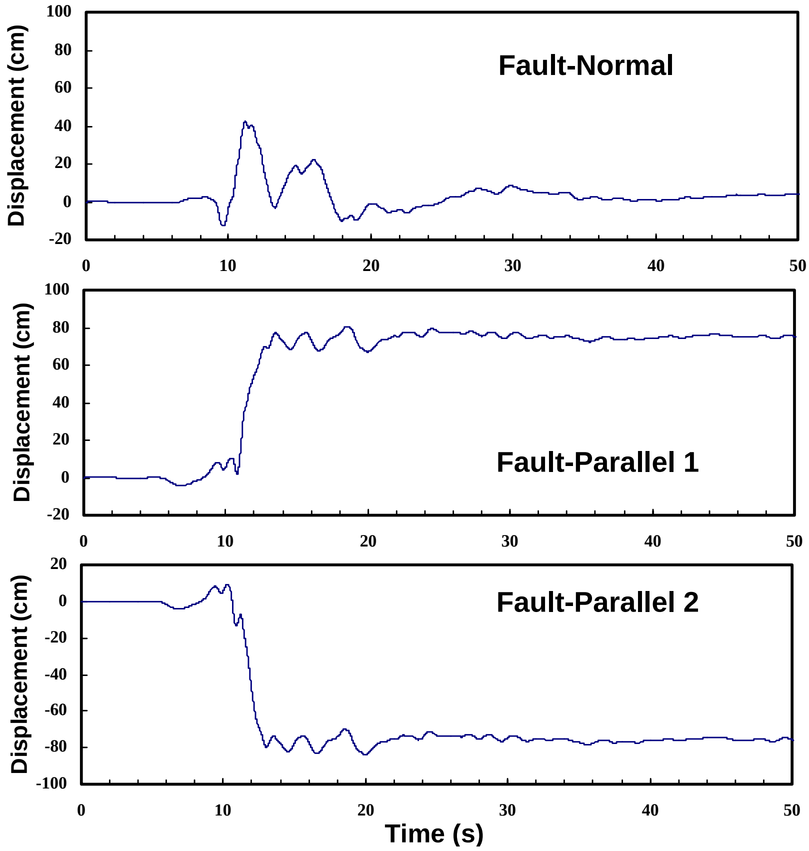

Fig. 7. Displacement histories of the simulated near-fault ground motion.

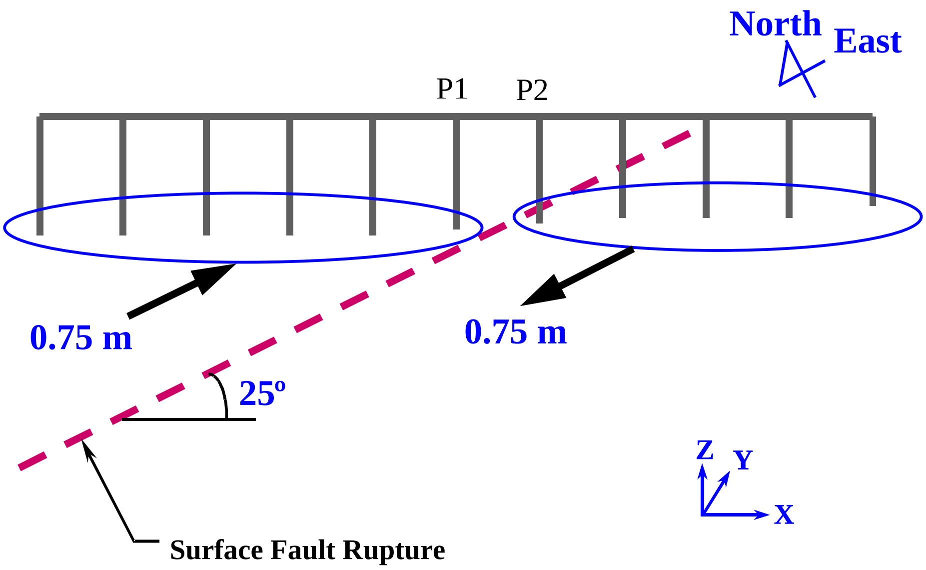

Fig. 8. Orientation of the surface fault rupture and direction of the residual ground movement.

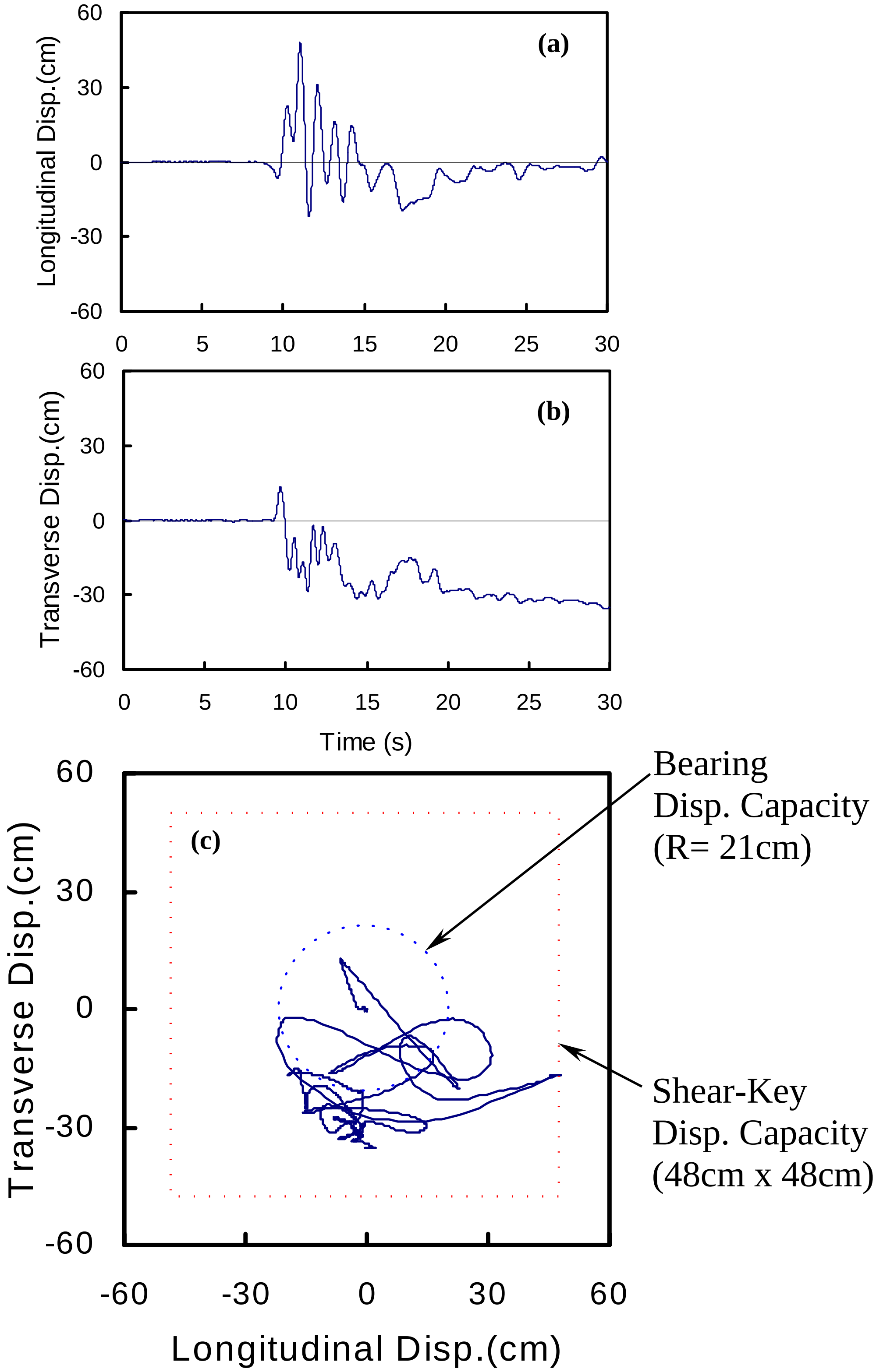

Fig. 9. Bearing displacement at the center pier under the Bolu ground motion: (a) longitudinal displacement history, (b) transverse displacement history, and (c) displacement path on the bearing surface.

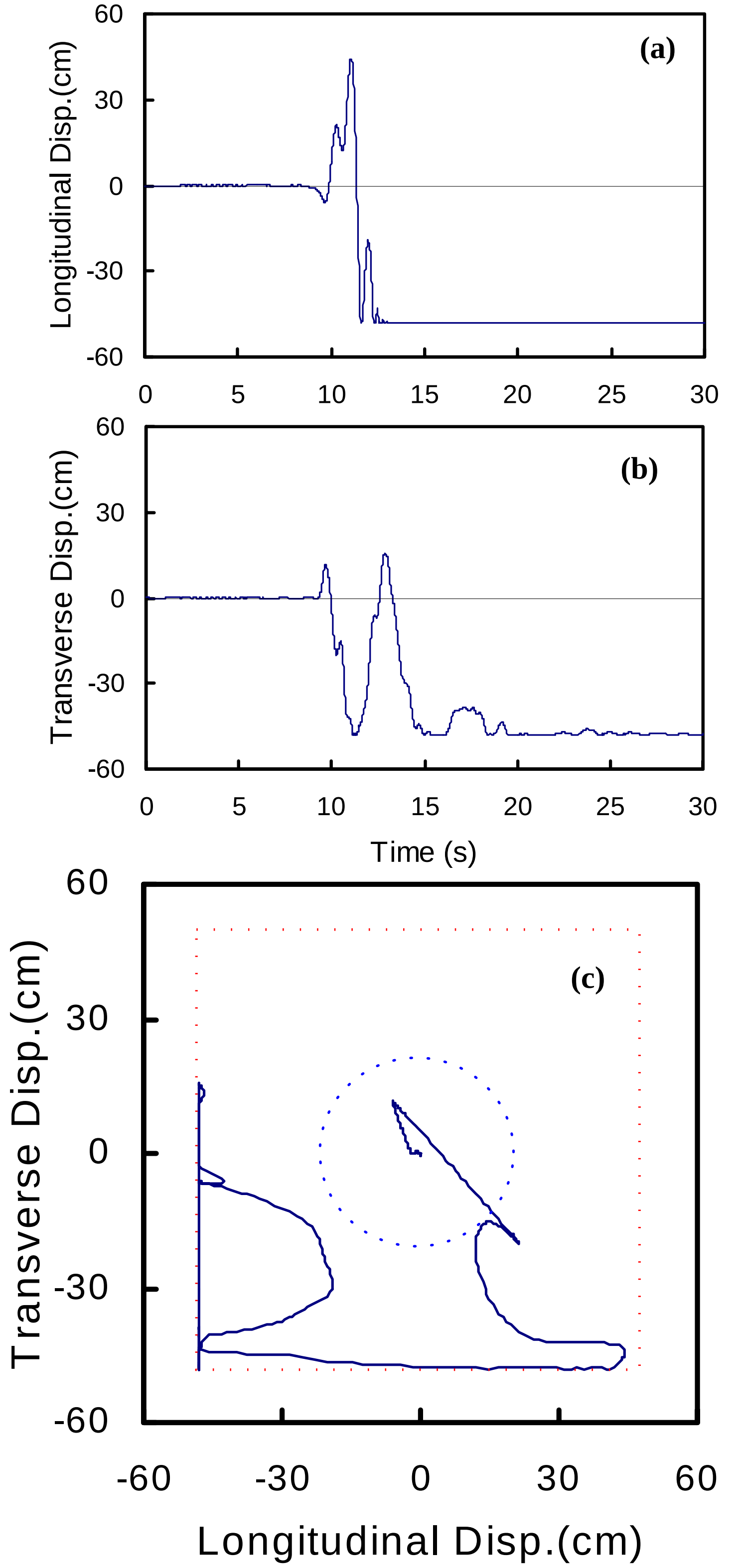

Fig. 10. Bearing displacement at Pier P1 (see Fig. 8) under the simulated near-fault ground motion: (a) longitudinal displacement history, (b) transverse displacement history, and (c) displacement path.

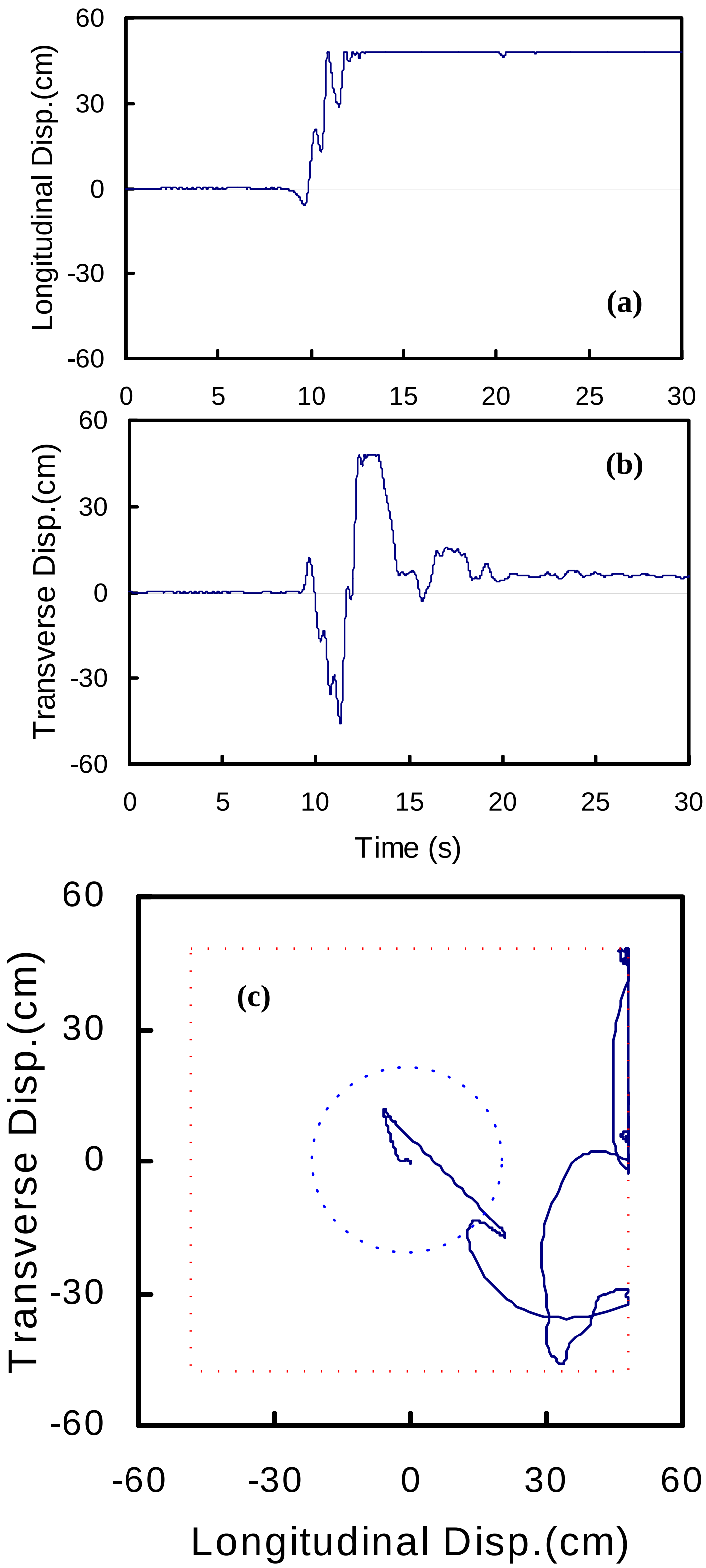

Fig. 11. Bearing displacement at Pier P2 (see Fig. 8) under the simulated near-fault ground motion: (a) longitudinal displacement history, (b) transverse displacement history, and (c) displacement path.

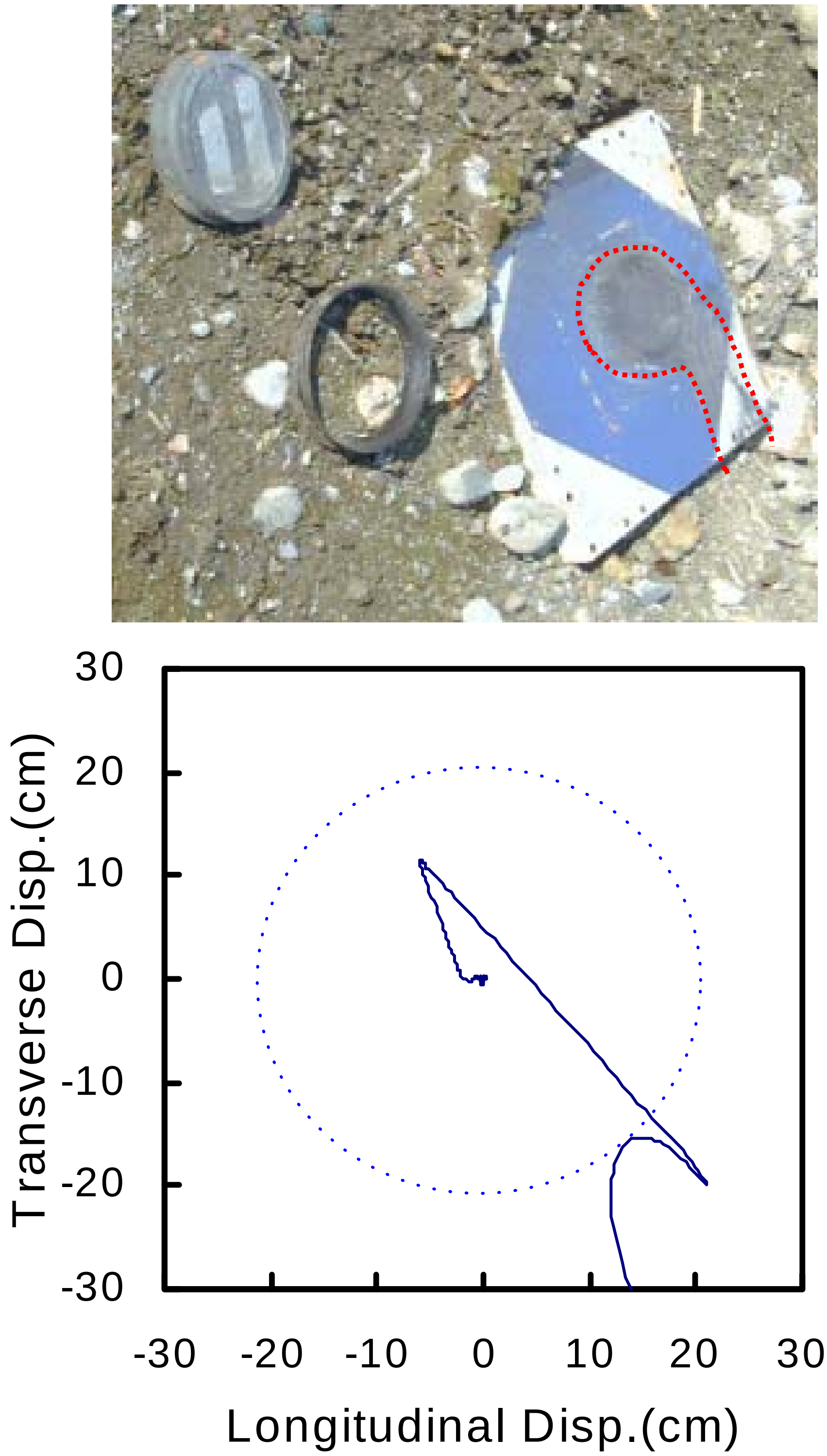

(a)

(b)

Fig. 12. Displacement path on the bearing surface during the initial stage of movement: (a) observed scoring trace on the bearing plate and (b) calculated displacement path from finite element analysis.